The Urokinase Receptor-Derived Peptide UPARANT Mitigates Angiogenesis in a Mouse Model of Laser-Induced Choroidal Neovascularization

Maurizio Cammalleri,[1] Massimo Dal Monte,[1] Filippo Locri,[1] Liliana Lista,[2] Monica Aronsson,[3] Anders Kvanta,[3] Dario Rusciano,[4] Mario De Rosa,[5] Vincenzo Pavone,[2] Helder André,[3] and Paola Bagnoli[1]

[1]Department of Biology, University of Pisa, Pisa, Italy
[2]Department of Chemical Sciences, University of Napoli Federico II, Napoli, Italy
[3]Department of Clinical Neurosciences, Section of Ophthalmology and Vision, St. Erik Hospital, Karolinska Institute, Stockholm, Sweden
[4]Sooft Italia Spa, Montegiorgio, Italy
[5]Department of Experimental Medicine, Second University of Napoli, Napoli, Italy

Correspondence: Paola Bagnoli, Department of Biology, University of Pisa, Via San Zeno, 31, 56127, Pisa, Italy;
paola.bagnoli@unipi.it.

MC, MDM, HA, and PB contributed equally to the work presented here and should therefore be regarded as equivalent authors.

Submitted: November 27, 2015
Accepted: April 3, 2016

Citation: Cammalleri M, Dal Monte M, Locri F, et al. The urokinase receptor-derived peptide UPARANT mitigates angiogenesis in a mouse model of laser-induced choroidal neovascularization. *Invest Ophthalmol Vis Sci*. 2016;57:2600–2611. DOI:10.1167/iovs.15-18758

Purpose. A mouse model of age-related macular degeneration (AMD) was used to investigate the anti-angiogenic and anti-inflammatory role of UPARANT in laser-induced choroidal neovascularization (CNV).

Methods. Choroidal neovascularization was induced by laser photocoagulation, and UPARANT was intravitreally injected. Some experiments were also performed after either intravitreal injection of anti-VEGF drugs or systemic administration of UPARANT. Immunohistochemistry using CD31 antibodies was used to evaluate the area of CNV. Evans blue dye extravasation was quantitatively assessed. Transcripts of markers of outer blood retinal barrier were measured by quantitative RT-PCR, also used to evaluate angiogenesis and inflammation markers. Western blot was used to determine levels of transcription factors encoding genes involved in angiogenesis and inflammation. Levels of urokinase-type plasminogen activator (uPA), its receptor (uPAR), and formyl peptide receptors (FPRs) were determined at the transcript and the protein level.

Results. Intravitreal UPARANT reduced the CNV area and the leakage from the choroid. The uPA/uPAR/FPR system was upregulated in CNV, but was not influenced by UPARANT. UPARANT recovered laser-induced upregulation of transcription factors encoding angiogenic and inflammatory markers. Accordingly, angiogenic and inflammatory factors were also reduced. UPARANT as compared to anti-VEGF drugs displayed similar effects on CNV area.

Conclusions. UPARANT mitigates laser-induced CNV by inhibiting angiogenesis and inflammation through an action on transcription factors encoding angiogenesis and inflammatory genes. The finding that UPARANT is effective against CNV may help to establish uPAR and its membrane partners as putative targets in the treatment of AMD.

Keywords: AMD, angiogenic factors, inflammatory factors, transcription factors

The leading cause for vision loss in the Western world is attributed to age-related macular degeneration (AMD),[1] of which neovascular AMD (nAMD) affects nearly two thirds of advanced AMD patients.[2] The imbalance in a multitude of angiogenic and inflammatory factors, under the control of hypoxia-dependent and -independent transcription factors,[3–5] leads to choroidal neovascularization (CNV) with invasion of the subretinal space by the newly formed vessels and leakage from the choroid.[3]

Retinal pigment epithelium plays a primary role in maintaining the outer blood retinal barrier (oBRB), and RPE cells are a major source of angiogenic and inflammatory factors.[3] Among these, VEGF plays a crucial role in CNV, and the recent availability of anti-VEGF drugs has represented a step forward in the treatment of nAMD.[6] However, the systemic safety of repeated injections may pose some concerns,[7] and the long-term benefits of anti-VEGF drugs can be limited by their loss of efficacy over time.[8] In addition, the multifactorial pathogenesis of nAMD[9] may cause some resistance to anti-VEGF therapies.[10] Thus, the identification of therapeutic approaches targeting novel pathways is actively pursued by basic research.[11]

Among several pathways known to be involved in angiogenic processes, the system formed by urokinase-type plasminogen activator (uPA) and its receptor (uPAR) is particularly attractive as it is a major player in VEGF-induced angiogenesis.[12] Interestingly, uPA and uPAR are localized to RPE and endothelial cells of the choroid.[13,14] In addition, the uPAR system is upregulated in rodent models of CNV, and its inhibition by

uPAR antagonists reduces CNV,[14–16] although the underlying mechanisms are not well understood.

Being devoid of intracellular domains, uPAR activates intracellular signaling cascades by lateral interactions with other components of the cellular membrane, including formyl peptide receptors (FPRs).[17] Formyl peptide receptors belong to a family of transmembrane G protein–coupled receptors that regulate the production of angiogenic and inflammatory factors through the modulation of transcription factors including hypoxia-inducible factor (HIF)-1, signal transducer and activator of transcription factor 3 (STAT3), nuclear factor kB (NF-kB), and cAMP response element binding protein (CREB).[18–20]

Among peptide inhibitors of uPAR, the tetrapeptide Ac-L-Arg-Aib-L-Arg-L-Cα(Me)Phe-NH_2, named UPARANT, displays lasting resistance to enzymatic digestion and high stability in blood and plasma; it strongly inhibits endothelial cell migration and proliferation by interfering with the complex cross talk between uPAR and FPRs.[21] In vitro, UPARANT reduces capillary sprout formation, whereas in vivo, it inhibits VEGF-induced vascularization in a rabbit corneal pocket assay and recovers retinal neovascularization, inner BRB leakage, and visual dysfunction in a mouse model of oxygen-induced retinopathy (OIR).[21,22]

In the current study, we addressed UPARANT's efficacy in a mouse model of laser-induced CNV. In this model, a thermal insult disrupts Bruch's membrane, allowing for an ingrowth of newly formed choroidal blood vessels into the subretinal compartment.[23,24] The laser-induced CNV model is one of the best models currently used to mimic the pathologic mechanisms in nAMD, although some differences in the chorioretinal environment and in the disease state (acute versus chronic) have been evidenced between mice and humans.[25] In the mouse model, we evaluated the effectiveness of UPARANT in inhibiting laser-induced CNV. In addition, we evaluated uPAR pathway involvement in CNV and whether the effects of UPARANT are mediated through the uPA/uPAR system. Finally, we assessed the effects of UPARANT on transcription factors involved in angiogenesis and inflammation and their markers. Overall, our data demonstrate that UPARANT is effective against CNV and suggest the uPAR system as a putative target in the treatment of nAMD.

Materials and Methods

The PBS was from Gibco (Paisley, UK). Bevacizumab and the protease and the phosphatase inhibitor cocktails were obtained from Roche Applied Science (Indianapolis, IN, USA). The recombinant mouse VEGF-R1/Flt-1 Fc chimera protein was from R&D Systems (Minneapolis, MN, USA). The RNeasy Mini, QuantiTect Reverse Transcription, and SYBR Green PCR kits were purchased from Qiagen, Inc. (Valencia, CA, USA). The primary antibody directed to CD31 was obtained from BD Biosciences Pharmingen (San Diego, CA, USA). The secondary antibody Alexa Fluor 546 was from Molecular Probes (Eugene, OR, USA). The primary antibodies (Supplementary Table S1) and the horseradish peroxidase (HRP)–conjugated secondary antibodies were from Santa Cruz Biotechnologies, Inc. (Santa Cruz, CA, USA). Polyvinylidene difluoride (PVDF) membranes were obtained from Bio-Rad Laboratories, Inc. (Hercules, CA, USA). The enhanced chemiluminescence reagent was from Millipore Corp. (Billerica, MA, USA). The ELISA kit for the detection of uPA was from LifeSpan BioSciences (Seattle, WA, USA). All other chemicals, including primary antibody directed to β-actin, were obtained from Sigma-Aldrich Corp. (St. Louis, MO, USA).

UPARANT Succinate

The angiogenesis inhibitor UPARANT, Ac-Arg-Aib-Arg-α(Me)Phe-NH_2, CAS NR 1006388-38-0, was synthesized as previously described.[21] Recently, it was produced as succinate salt (Boccelli S, unpublished data, 2015) that was used in the present study. Composition of the test item was peptide content of 78.6% (as 100% − [succinate + acetate + water]%); succinic acid content 17.6%; acetic acid content 0.85%; water content 2.9%. Purity assessment by RP-HPLC was 99.3%. Each individual unknown impurity was <0.5%. Sum of total impurities was 0.7%. For simplicity, UPARANT succinate, used in this work, will be henceforth referred to as UPARANT.

Animals and CNV Induction

Choroidal neovascularization lesions were induced in 6- to 8-week-old C57BL/6J mice (Charles River, Cologne, Germany) as previously described.[23] Thirty-seven mice underwent four lesions per eye for immunohistochemical studies, and 63 mice nine lesions per eye for molecular studies. On day 15 after CNV lesion induction, mice were euthanized and both eyes enucleated and cleared from surrounding tissues. All animals were treated in accordance with the ARVO Statement for the Use of Animals in Ophthalmic and Vision Research, and Stockholm's Committee for Ethical Animal Research approved all study protocols.

Pharmacologic Treatments

On day four after induction of CNV, mice were randomly distributed into three groups, and both eyes were intravitreally injected with 1 μL of vehicle (PBS) or UPARANT (dissolved in PBS) at both 4 mg mL^{-1} and 12 mg mL^{-1}. For clarity, UPARANT concentrations in succinate salt are equivalent to 9.43 and 3.14 mg mL^{-1} of active UPARANT peptide. All mice were subsequently treated according to their grouping on days 4, 8, and 12 after laser induction.

To compare the effects of UPARANT with those of anti-VEGF drugs, bevacizumab (1 μL) at 1.25 mg mL^{-1} and a recombinant mouse VEGF-R1 Fc chimera protein (1 mg mL^{-1}, 1 μL) were intravitreally injected in both eyes of mice with four laser CNV lesions, following the same treatment scheme as used for UPARANT.

Immunohistochemistry

Immunohistochemistry for CD31, an endothelial cell marker, was performed on flattened RPE-choroid complexes 15 days after laser exposure. Briefly, eyeballs were fixed overnight in 4% paraformaldehyde in 0.1 M phosphate buffer (PB), transferred to 25% sucrose in 0.1 M PB, and stored at 4°C. Fixed eyes were dissected at the equator to obtain posterior sclerochoroidal eyecups, and the neural retina was removed. The RPE-choroid complexes were rinsed in 0.1 M PB and incubated for 72 hours at 4°C in rat anti-mouse CD31 (1:50 in 0.1 M PB containing 0.5% Triton X-100). The RPE-choroidal complexes were incubated subsequently for 48 hours at 4°C with Alexa Fluor 546–conjugated secondary antibody (1:200 in 0.1 M PB) followed by rinsing in 0.1 M PB. Four radial incisions were made in the RPE-choroid-sclera complexes, flat-mounted on gelatin-coated glass slides, and coverslipped with a 0.1 M PB-glycerin mixture. Images of the tissue samples were acquired with a microscope equipped with epifluorescence (Eclipse E800; Nikon, Amsterdam, The Netherlands) through a digital photocamera (DS-Fi1c; Nikon). An image-editing software (Adobe Photoshop CS3; Adobe Systems, Inc., Mountain

View, CA, USA) was used to measure the size of hyperfluorescent areas corresponding to CNV lesions.

Extravasation Assay

Mice with nine lesions per eye (or control mice) were anesthetized using ketamine (90 mg kg^{-1}) and xylazine (15 mg kg^{-1}). Five hundred microliters of Evans blue dye (0.5% in PBS) were injected into the left ventricle of each animal and allowed to circulate for 10 minutes. The animals were euthanized, and the eyes were dissected from the surrounding tissues. The dye content of the eyes was then extracted by formamide overnight at 65°C and read at 620 nm using a plate reader (Infinite F200; Tecan Trading AG, Grödig, Austria).

Quantitative RT-PCR

Eyeballs used in molecular studies (quantitative RT-PCR, ELISA, and Western blot analysis) were immediately microdissected to obtain RPE-choroid complexes, frozen in liquid nitrogen, and stored at –80°C until use. To perform quantitative real-time RT-PCR (qPCR) experiments, three samples, each containing one RPE-choroid complex, were used for each experimental condition. Total RNA was extracted using an isolation kit (RNeasy Mini Kit; Qiagen, Inc.), purified, resuspended in RNase-free water, and quantified using a fluorometer (Invitrogen, Carlsbad, CA, USA). First-strand cDNA was generated from 1 μg total RNA (Qiagen, Inc.).

Gene expression was evaluated using an SYBR Green PCR Kit (Qiagen, Inc.). Quantitative real-time RT-PCR primer sets for oBRB markers, the uPA/uPAR/FPR system, angiogenic factors, and inflammatory markers were chosen to hybridize to unique regions of the appropriate gene sequence (Supplementary Table S2 for complete list of assayed genes and primers). Amplification efficiency was close to 100% for each primer pair (Opticon Monitor 3 software; Bio-Rad Laboratories, Inc.). Target genes were assayed concurrently with ribosomal protein (Rp)L13a, a constitutively expressed gene encoding a ribosomal protein. Samples were compared using the relative threshold cycle (Ct method). The increase or decrease (fold change) was determined relative to control mice after normalization to RpL13a. All reactions were performed in triplicate.

Enzyme-Linked Immunosorbent Assay

Quantification of uPA protein levels was determined in protein extracts containing soluble proteins also used for Western blot analysis (see below). The ELISA plate was evaluated spectrophotometrically (Microplate Reader 680 XR; Bio-Rad Laboratories, Inc.). Data were expressed as picograms of uPA per milligram of protein. All experiments were run in duplicate.

Western Blot Analysis

To perform Western blot experiments, three samples, each containing two RPE-choroid complexes from two independent mice, were used for each experimental condition. Retinal pigment epithelium–choroid complexes were sonicated in 10 mM Tris-HCl (pH 7.6) containing 5 mM EDTA, 3 mM EGTA, 250 mM sucrose, and protease and phosphatase inhibitor cocktails and were centrifuged at 22,000*g* for 30 minutes at 4°C. The supernatants, containing cytosolic and interstitial proteins, were used to detect soluble proteins. Membrane-bound proteins were isolated from the pellets by resuspension in 20 mM HEPES, pH 7.4, containing 150 mM NaCl, 5 mM EDTA, 3 mM EGTA, 4 mg mL^{-1} *n*-dodecyl-β-maltoside, protease and phosphatase inhibitor cocktails and were clarified by centrifugation at 22,000*g* for 30 minutes at 4°C. Protein concentration was determined using a fluorometer (Qubit; Invitrogen). Aliquots of each sample containing equal amounts of protein (30 μg) were subjected to SDS-PAGE, and β-actin was used as the loading control. The gels were transblotted onto PVDF membrane, and the blots were blocked in 3% skim milk for 1 hour at room temperature, followed by incubation overnight at 4°C with antibodies as indicated in Supplementary Table S1. Finally, blots were incubated for 1 hour at room temperature with HRP-conjugated secondary antibodies (1:5000) and developed with enhanced chemiluminescence reagent. Images were acquired (ChemiDoc XRS+; Bio-Rad Laboratories, Inc.), and optical density (OD) of the bands was evaluated (Image Lab 3.0 software; Bio-Rad Laboratories, Inc.). The data were normalized to the corresponding OD of β-actin, STAT3, NF-kB, or CREB, as appropriate. All experiments were performed in duplicate.

Data Analysis

Statistical significance was evaluated using ANOVA, followed by Newman-Keuls multiple comparison posttest. The results are expressed as mean ± SEM of the indicated *n* values (Prism 5; GraphPad Software, San Diego, CA, USA). Differences with $P < 0.05$ were considered significant.

Results

UPARANT Mitigates CNV

In preliminary experiments, we evaluated maximum tolerated dose (MTD) to determine UPARANT toxicity (Supplementary Fig. S1). Evidence of abnormalities in the choroid, RPE, or retina were observed at 108 mg mL^{-1}. Such data indicated that doses of 4 and 12 mg mL^{-1} would be considerably below the MTD for UPARANT after intravitreal injection. In addition, evaluation of transcript levels of apoptotic markers displayed no elevation in laser-induced CNV eyes with doses of both 4 and 12 mg mL^{-1} (Supplementary Fig. S1). In agreement, we opted to perform the following experiments using the doses below the extrapolated MTD.

In order to evaluate choroidal angiogenesis, blood vessels were immunostained with CD31. For this purpose, the area of CNV was quantified in flat-mounts of RPE-choroid complexes from vehicle-treated mice and those that received UPARANT. As compared to choroids of vehicle-treated mice (Fig. 1A), the area of laser-induced CNV lesions was evidently reduced in choroids of UPARANT-treated mice (Figs. 1B, 1C). Quantitative analysis confirmed that UPARANT dose-dependently reduced the CNV area (Fig. 1F). In particular, UPARANT at 4 mg mL^{-1} reduced the CNV area by approximately 40% ($P < 0.01$), while UPARANT at 12 mg mL^{-1} reduced the CNV area by approximately 60% ($P < 0.001$).

To evaluate the effectiveness of UPARANT in respect to that of anti-VEGF drugs known to be effective in mouse models of CNV and OIR,[26–28] we compared the effects of UPARANT on the CNV area with those of either bevacizumab (1.25 mg mL^{-1}; Fig. 1D) or a recombinant mouse VEGF-R1 Fc chimera protein (1 mg mL^{-1}; Fig. 1E). As shown in Figure 1F, the effects of anti-VEGF drugs on CNV did not differ from those of UPARANT at 4 mg mL^{-1}, yet were considerably elevated when compared to UPARANT at 12 mg mL^{-1}. In particular, the CNV area was reduced by bevacizumab and the recombinant mouse VEGF-R1 Fc chimera protein by approximately 36% and 47%, respectively ($P < 0.01$), when compared to a range reduction of CNV area by 60% after UPARANT treatment at 12 mg mL^{-1}.

Breakdown of the oBRB[29] and albumin extravasation due to reduced levels of barrier proteins[30] have been associated with

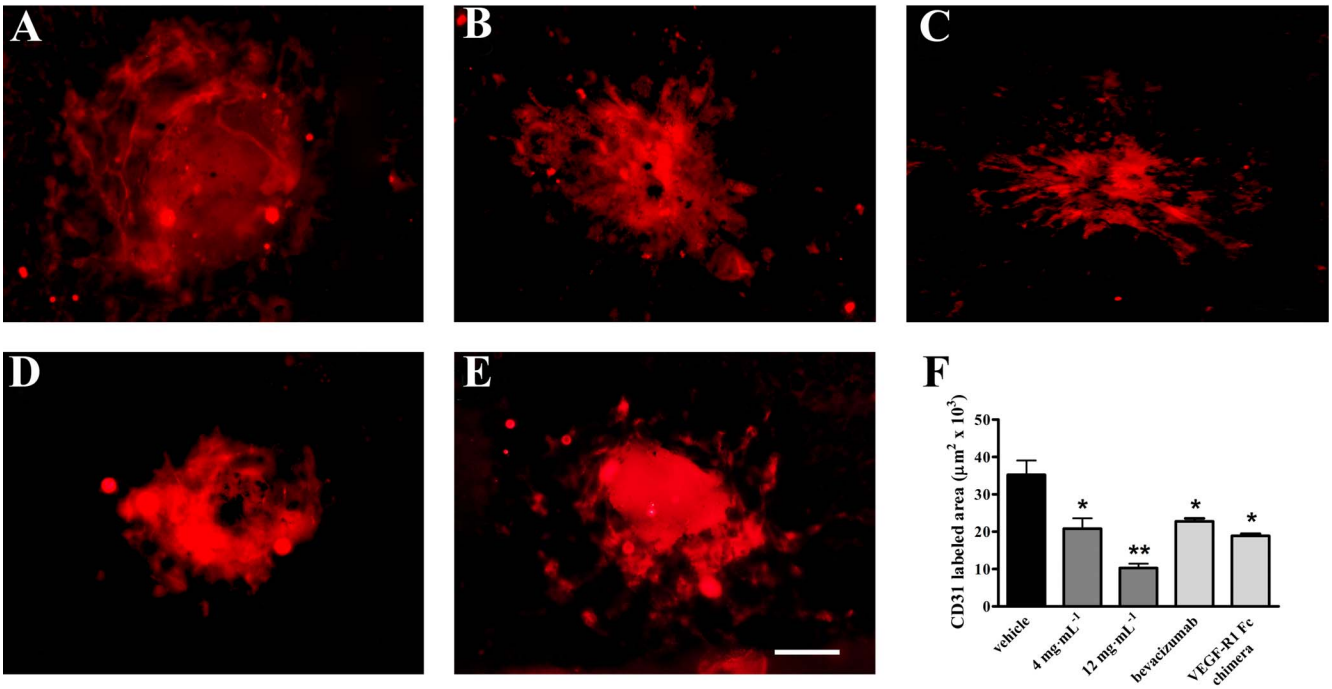

Figure 1. UPARANT ameliorates CNV. Choroidal neovascularization was detected using an antibody directed to CD31 in flat-mounts of RPE-choroid complexes in mice treated with vehicle (**A**) or with UPARANT at 4 mg mL^{-1} (**B**) or 12 mg mL^{-1} (**C**), and with bevacizumab at 1.25 mg mL^{-1} (**D**) or a recombinant mouse VEGF-R1 Fc chimera protein at 1 mg mL^{-1} (**E**). *Scale bar*: 100 μm. (**F**) Quantitative analysis of CNV area. *Bars* indicate the average CNV area in each group (*$P < 0.01$ and **$P < 0.001$ versus vehicle-treated; ANOVA). Each column represents the mean ± SEM of data from six RPE-choroid complexes.

CNV. As shown in Figure 2A, UPARANT dose-dependently reduced laser-induced leakage from the choroid as evaluated by quantitative assessment of Evans blue dye extravasation. Evans blue dye leakage was increased by approximately 2.0-fold ($P < 0.05$) by laser treatment, and 4 mg mL^{-1} UPARANT prevented this increase. Notably, 12 mg mL^{-1} UPARANT reduced Evans blue dye leakage to a level close to 12% lower than that in controls ($P < 0.05$). Furthermore, laser treatment reduced the transcript levels of oBRB markers[31] occludin (Fig. 2B), claudin-1 (Fig. 2C), and ZO-1 (Fig. 2D) by approximately 56% ($P < 0.001$), 46% ($P < 0.01$), and 60% ($P < 0.001$), respectively. After UPARANT at 4 mg mL^{-1}, the levels of occludin, claudin-1, and ZO-1 were, in order, approximately 34% ($P < 0.01$), 36% ($P < 0.05$), and 39% ($P < 0.001$) lower than controls. Markedly, 12 mg mL^{-1} UPARANT recovered the levels of claudin-1 to those of controls, while the levels of occludin were approximately 15% ($P < 0.05$) and ZO-1 approximately 20% ($P < 0.01$) lower than controls.

Additionally, we assessed whether UPARANT could reach therapeutic ocular levels after systemic administration. Using VEGF transcripts as a marker (Supplementary Fig. S2), we denoted that 1 mg of subcutaneously administered UPARANT could reduce VEGF mRNA to levels comparable to 4 mg mL^{-1} administered intravitreally. These data indicate systemic activity of UPARANT in ocular angiogenesis.

UPARANT Does Not Directly Affect the uPA/uPAR System

We investigated the involvement of the uPAR pathway in CNV and whether the effects of UPARANT could be directly affecting the uPA/uPAR system. As illustrated in Figure 3, laser treatment did not affect uPA transcript (Fig. 3A), while it increased the level of uPA protein (Fig. 3B) by 2.1-fold ($P < 0.001$). No effects of UPARANT on uPA transcript or protein could be observed (Figs. 3A, 3B). In addition, uPAR transcript (Fig. 4A) increased in response to laser treatment by approximately 2.1-fold and uPAR protein (Fig. 4F) by approximately 2.5-fold ($P < 0.001$). Neither FPR transcripts nor FPR proteins were affected by laser treatment (Figs. 4B–D, 4G, 4I), with the exception of FPR2 proteins, which were increased by 2.4-fold (Fig. 4H; $P < 0.001$). At none of the doses administered was UPARANT found to influence the expression of uPAR or FPRs at both transcript and protein levels. Representative blots depicting the effects of UPARANT on uPA, uPAR, and FPR at protein levels are shown in Figure 4E.

UPARANT Downregulates Levels of Transcription Factors

The effects of UPARANT on the levels of transcription factors involved in CNV[3–5,23] were investigated. As displayed in Figure 5, laser treatment increased the levels of HIF-1α by approximately 4.2-fold ($P < 0.001$) and enhanced the phosphorylation of STAT3 at Tyr^{705}, NF-kB p65 at both Ser^{276} and Ser^{536}, and CREB at Ser^{133} by approximately 28.6-, 6.1-, 4.4-, and 3.3-fold, respectively ($P < 0.001$). UPARANT reduced transcription factors with a trend toward recovering their control levels. Upon 4 mg mL^{-1} UPARANT, the levels of HIF-1α, pSTAT3 (Tyr^{705}), pNF-kB p65 (Ser^{276}), pNF-kB p65 (Ser^{536}), and pCREB (Ser^{133}) were approximately 2.5- ($P < 0.001$), 10.0- ($P < 0.01$), 2.4- ($P < 0.001$), 2.6- ($P < 0.001$), and 2.1-fold ($P < 0.001$) higher than those measured in controls, respectively. Upon 12 mg mL^{-1} UPARANT, the levels of HIF-1α, pNF-kB p65 (Ser^{536}), and pCREB (Ser^{133}) did not statistically differ from those measured in controls, while the levels of pSTAT3 (Tyr^{705}) and pNF-kB p65 (Ser^{276}) were approximately 6.7- and 2.0-fold higher than those measured in controls, respectively ($P < 0.05$). Following 12 mg mL^{-1} UPARANT, the levels of pSTAT3 (Tyr^{705}) and pNF-kB p65 (Ser^{276}) were 77% and 67% lower than in vehicle-treated mice, respectively ($P < 0.001$).

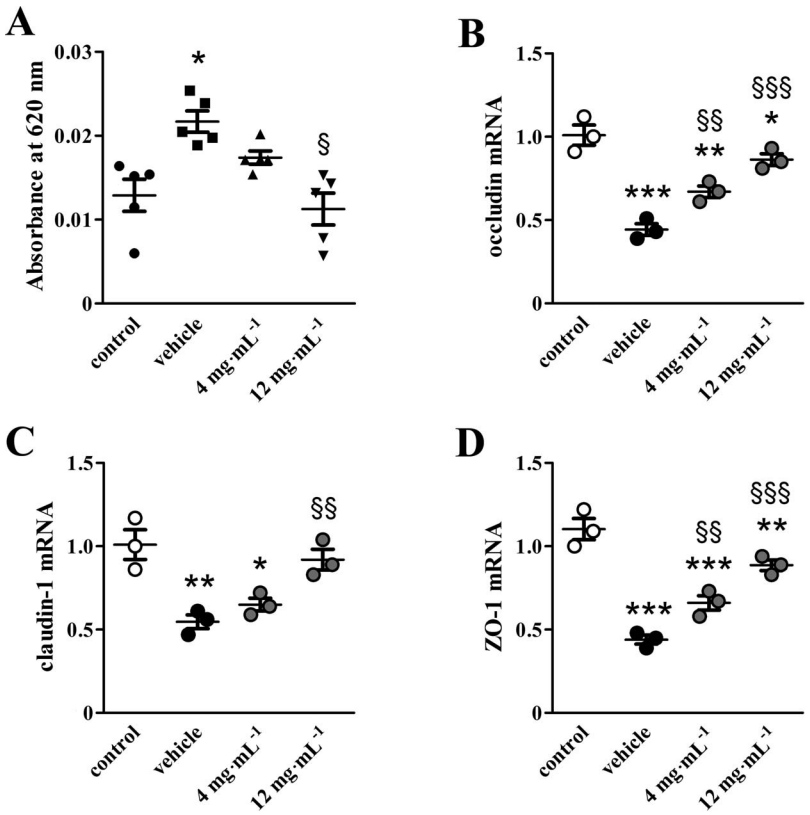

FIGURE 2. UPARANT reduces oBRB damage in CNV. (**A**) Laser-induced leakage from the choroid was evaluated by quantitative assessment of Evans blue dye extravasation. Laser treatment increased Evans blue dye extravasation. UPARANT reduced the extravasation with a trend toward recovering control levels. (**B–D**) Transcript levels of the oBRB markers occludin (**B**), claudin-1 (**C**), and ZO-1 (**D**) were evaluated by qPCR. Data were analyzed by the formula $2^{-\Delta\Delta CT}$ using RpL13a as internal standard. Laser treatment decreased barrier proteins. UPARANT prevented the reduction with a trend toward recovering control levels ($^{*}P < 0.05$, $^{**}P < 0.01$, and $^{***}P < 0.001$ versus control; $^{\S}P < 0.05$, $^{\S\S}P < 0.01$, and $^{\S\S\S}P < 0.001$ versus vehicle-treated; ANOVA). Data are presented as scatter plots. Each plot represents the mean ± SEM of data from five (**A**) or three (**B–D**) independent samples, each containing 1 RPE-choroid complex.

UPARANT Reduces the Expression of Angiogenic Factors

The transcript levels of several angiogenic factors, including VEGF, insulin-like growth factor (IGF)-1, angiopoietin (Ang)-2, FGF-2, and platelet-derived growth factor (PDGF)-B, are increased in mouse models of CNV.[32–35] The effects of UPARANT on angiogenic factor transcripts were investigated. As illustrated in Figure 6, after laser treatment, the levels of VEGF, IGF-1, Ang-2, FGF-2, and PDGF-B were increased by approximately 1.9-, 1.6-, 2.1-, 2.1-, and 1.9-fold, respectively ($P < 0.001$). UPARANT reduced angiogenic factors, with a trend toward recovering their control levels. Specifically, after UPARANT at 4 mg mL^{-1}, the levels of VEGF, IGF-1, Ang-2,

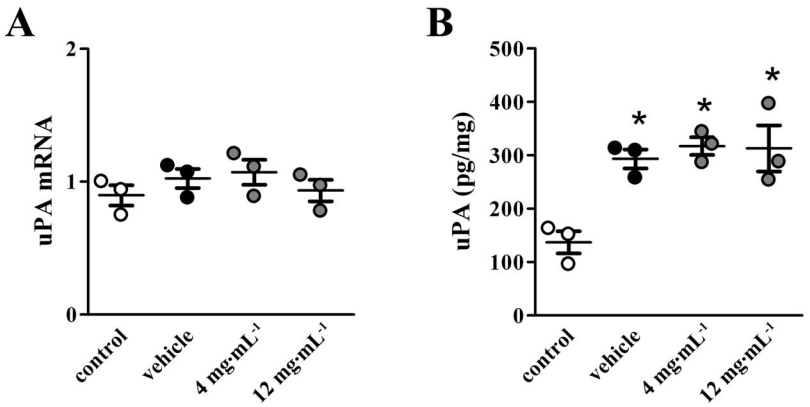

FIGURE 3. UPARANT does not affect uPA. (**A**) Transcript levels of uPA were evaluated by qPCR in RPE-choroid complexes of mice untreated or treated with vehicle or with UPARANT at 4 or 12 mg mL^{-1}. Data were analyzed by the formula $2^{-\Delta\Delta CT}$ using RpL13a as internal standard. (**B**) Protein levels of uPA were evaluated by ELISA. Laser treatment had no effects on uPA transcript, whereas it increased uPA protein. UPARANT had no effects on uPA levels ($^{*}P < 0.001$ versus control; ANOVA). Data are presented as scatter plots. Each plot represents the mean ± SEM of data from three independent samples, each containing one RPE-choroid complex.

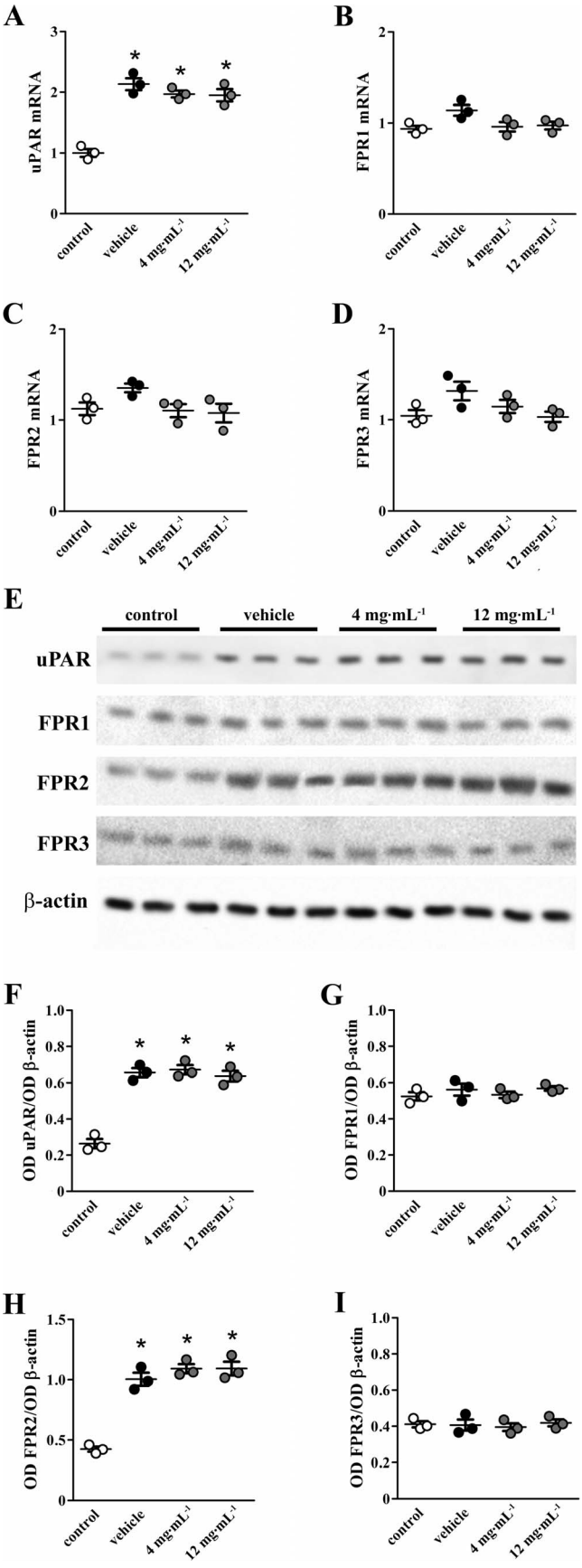

Figure 4. Regulation of uPAR and FPRs in CNV is independent of UPARANT. Transcript levels of uPAR (**A**), FPR1 (**B**), FPR2 (**C**), and FPR3 (**D**) were evaluated by qPCR in RPE-choroid complexes of mice untreated or treated with vehicle or with UPARANT at 4 or 12 mg mL^{-1}. Data were analyzed by the formula $2^{-\Delta\Delta CT}$ using RpL13a as internal standard. (**E**) Protein levels of uPAR and FPRs were evaluated by Western blot using β-actin as the loading control. (**F–I**) Densitometric analysis of the blots depicted in (**E**). Laser treatment increased uPAR transcript and protein. Neither FPR transcripts nor FPR proteins were affected by laser treatment with the exception of FPR2 protein. UPARANT had no effects on uPAR or FPR levels (*$P < 0.001$ versus control; ANOVA). Data are presented as scatter plots. Each plot represents the mean ± SEM of data from three independent samples, each containing one (**A–D**) or two (**F–I**) RPE-choroid complexes.

FGF-2, and PDGF-B were approximately 1.5- ($P < 0.01$), 1.4- ($P < 0.01$), 1.9- ($P < 0.001$), 1.9- ($P < 0.001$), and 1.5-fold ($P < 0.01$) higher than in controls, respectively. On the other hand, UPARANT at 12 mg mL^{-1} recovered the levels of VEGF, FGF-2, and PDGF-B that were not statistically different from those measured in controls. In contrast, the levels of IGF-1 and Ang-2 were approximately 1.2- ($P < 0.05$) and 1.4-fold ($P < 0.01$) higher than in controls, respectively, and approximately 24% and 30% lower than in vehicle-treated, respectively ($P < 0.01$). These results were further confirmed at the protein level for VEGF, Ang-2, and FGF-2 (Supplementary Fig. S3).

UPARANT Decreases the Expression of Inflammatory Factors

Choroidal neovascularization is characterized by an increase in transcript levels of several inflammatory factors, including IL-1β, IL-6, TNF-α, inducible nitric oxide synthase (iNOS), monocyte chemotactic protein (MCP)-1, and intracellular adhesion molecule (ICAM)-1.[36–39] To evaluate the effects of UPARANT on inflammatory factors, mRNA levels were determined and quantified. As depicted in Figure 7, after laser treatment, the levels of IL-1β, IL-6, TNF-α, iNOS, MCP-1, and ICAM-1 were increased by approximately 4.7-, 2.8-, 2.6-, 2.1-, 4.0-, and 3.7-fold, respectively ($P < 0.001$). Similar to the effects exerted on angiogenic factors, UPARANT reduced inflammatory transcripts, with a trend toward recovering their control levels. In particular, after UPARANT at 4 mg mL^{-1}, the levels of IL-1β, IL-6, TNF-α, iNOS, MCP-1, and ICAM-1 were approximately 3.5- ($P < 0.001$), 2.2- ($P < 0.01$), 1.6- ($P < 0.01$), 1.5- ($P < 0.05$), 3.1- ($P < 0.001$), and 2.9-fold ($P < 0.001$) higher than in controls, respectively. Markedly, 12 mg mL^{-1} UPARANT treatment statistically reduced the levels of TNF-α and iNOS to those of controls, while the levels of IL-1β, IL-6, MCP-1, and ICAM-1 were approximately 2.5- ($P < 0.001$), 1.7- ($P < 0.05$), 2.0- ($P < 0.01$), and 1.7-fold ($P < 0.01$) higher than in controls, respectively. These levels were approximately 46% ($P < 0.01$), 39% ($P < 0.01$), 50% ($P < 0.001$), and 55% ($P < 0.001$) lower than in vehicle-treated mice, respectively.

Discussion

In general, compared with VEGF-neutralizing antibodies or VEGF decoy soluble receptors (VEGF-traps), peptides such as UPARANT show several advantages, including considerably higher activity per unit mass, greater stability, reduced interactions with the immune system, and better tissue permeability.[40] The present study characterizes, we believe for the first time, the effects of UPARANT in a mouse model of laser-induced CNV that mimics the blinding disease AMD. UPARANT reduces CNV, likely through an action at uPAR cross talk with FPRs, by influencing transcription factors that regulate the expression of both angiogenic and inflammatory factors.

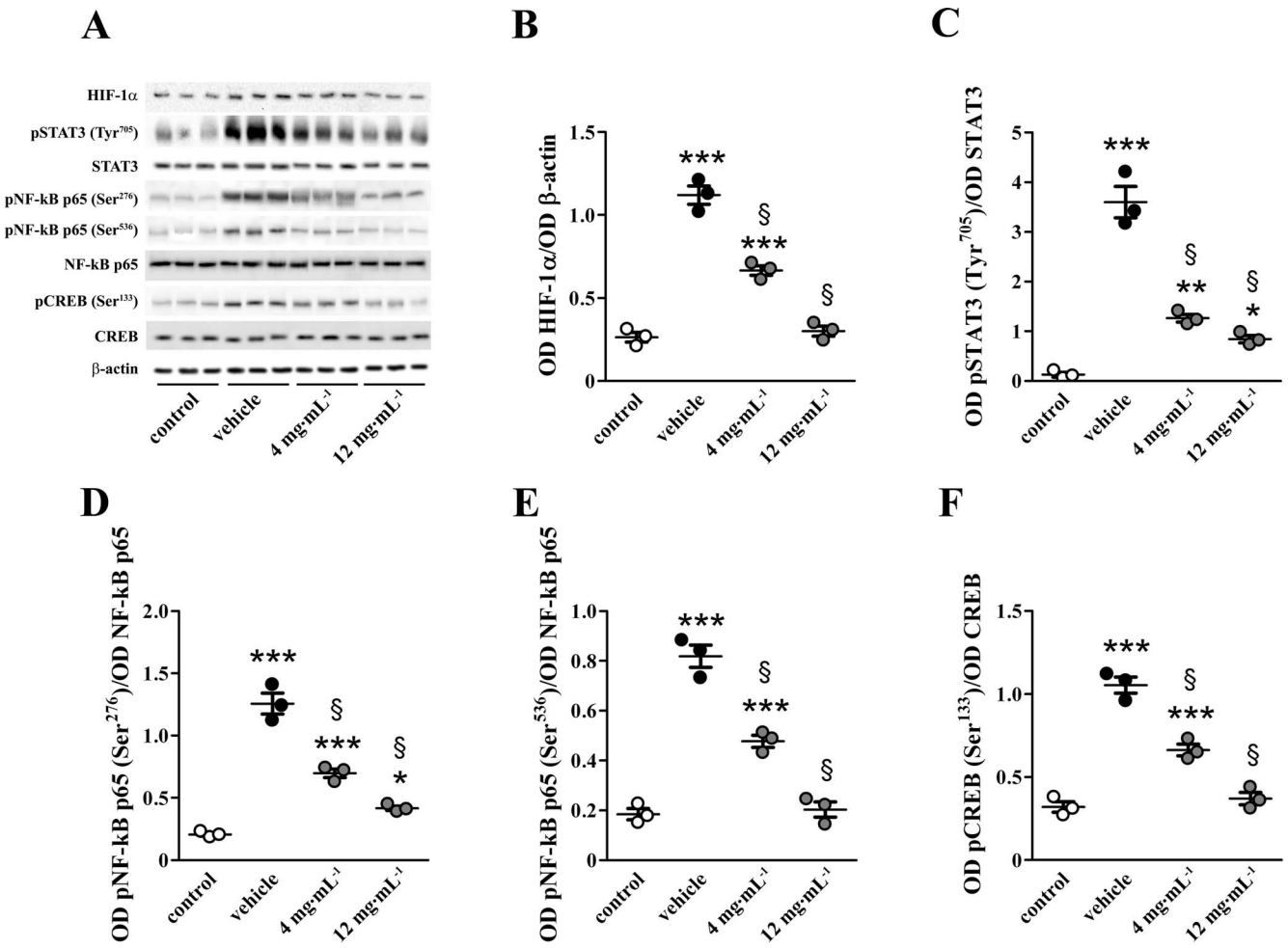

FIGURE 5. Downregulation of transcription factors by UPARANT. (**A**) Protein levels of HIF-1α, pSTAT3 (Tyr^{705}), STAT3, pNF-kB p65 (Ser^{276}), pNF-kB p65 (Ser^{536}), NF-kB p65, pCREB (Ser^{133}), and CREB were evaluated by Western blot analysis in RPE-choroid complexes of mice untreated or treated with vehicle or with UPARANT at 4 or 12 mg mL^{-1}. β-actin was used as the loading control. (**B–F**) Densitometric analysis of the blots depicted. Protein expression was relative to the loading control β-actin (HIF-1α), to STAT3 (pSTAT3 [Tyr^{705}]), to NF-KB p65 (pNF-kB p65 [Ser^{276}] and pNF-kB p65 [Ser^{536}]) or to CREB (pCREB [Ser^{133}]). Laser treatment increased transcription factors. UPARANT reduced transcription factors, with a trend toward recovering control levels (*$P < 0.05$, **$P < 0.01$, and ***$P < 0.001$ versus control; §$P < 0.001$ versus vehicle-treated; ANOVA). Data are presented as scatter plots. Each plot represents the mean ± SEM of data from three independent samples, each containing two RPE-choroid complexes from independent mice.

UPARANT Doses and Safety

UPARANT doses used in the present study are in the range of those previously reported in a mouse model of OIR.[22] Drugs delivered by intravitreal injections diffuse through the vitreous in order to reach the target tissues, being in part eliminated by anterior and posterior routes, thus decreasing their actual vitreal concentration.[41] Therefore, when injected into the posterior eye chamber, drugs need to be delivered at relatively high concentrations. This requirement is not a limit in the case of UPARANT. In fact, our results show that UPARANT MTD is 36 mg mL^{-1} (Supplementary Fig. S1), a dose one order of magnitude greater than the minimum effective dose used in the present study. Safety of UPARANT is further supported by the finding that apoptotic processes that characterize the choroid after laser treatment[42] are not significantly increased by the drug at any concentration.

UPARANT Effects on CNV

As shown by the present results, in a mouse model of laser-induced CNV, UPARANT ameliorates choroidal angiogenesis by reducing the CNV area and the leakage from the choroid. These findings further confirm the role of the uPA/uPAR system and its interactome in regulating angiogenic processes in the choroid.[43] In this respect, previous data demonstrating that uPA/uPAR system blockade reduces CNV not only in rodents,[14,44] but also in non-human primates,[45] suggest that this system may be a potential target to develop novel therapeutic interventions aimed to counteract choroidal neovascularization.

Recently, anti-VEGF drugs have been introduced to treat CNV.[46] There is evidence that VEGF acts as a major stimulator of CNV; however, additional pathways are also known to be involved in choroidal angiogenesis.[47] Inhibition of VEGF signaling alone is sufficient to decrease CNV, but a greater decrease of angiogenesis may be obtained by using drugs targeting multiple pathways,[48] indicating that a pharmacologic strategy aimed at inhibiting multiple angiogenic pathways may be a more desirable therapeutic approach. In this respect, the present data indicating that the multitarget molecule UPARANT is as effective (if not superior) when compared to anti-VEGF drugs in reducing CNV suggest that UPARANT may be of great value in the treatment of CNV.

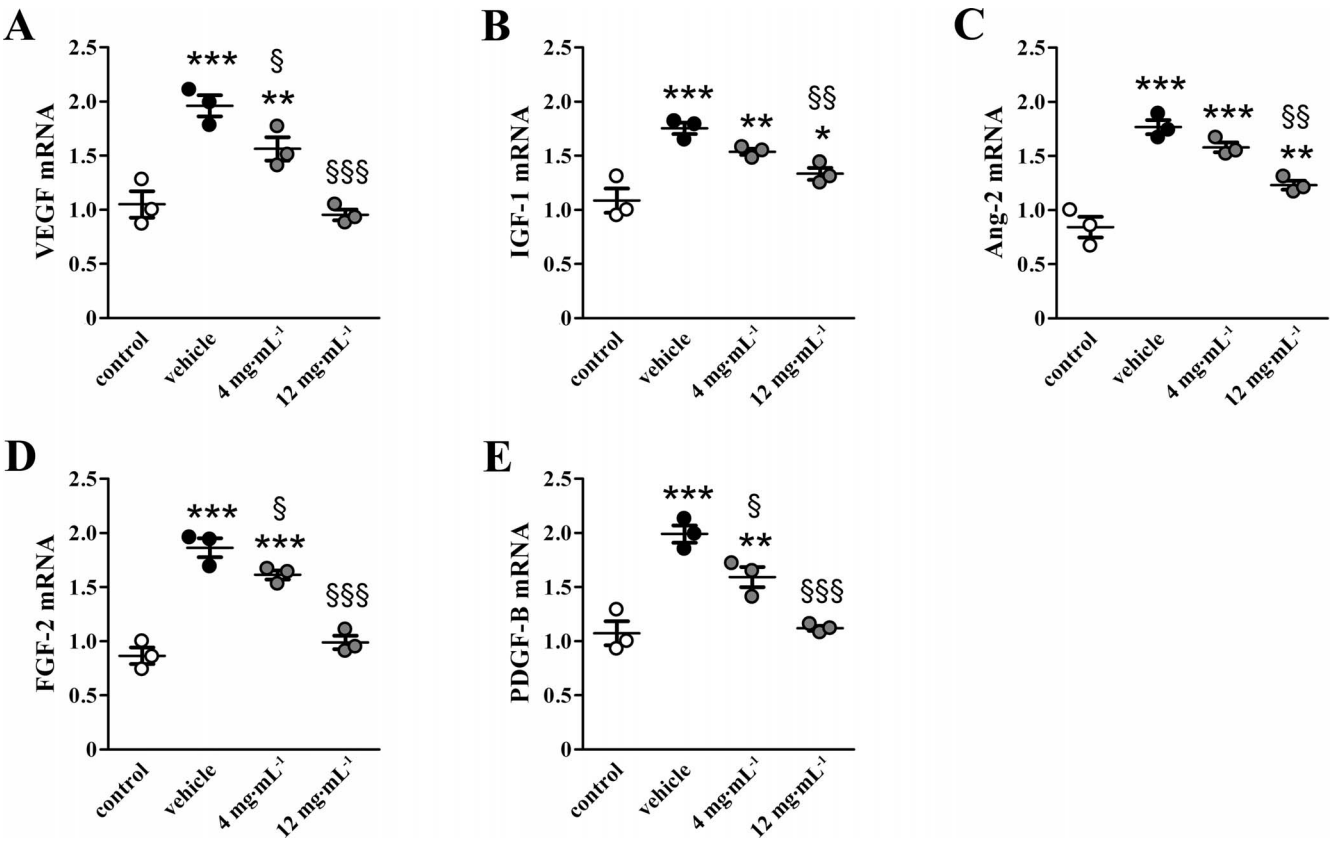

FIGURE 6. UPARANT downregulates angiogenic factors. Transcript levels of VEGF (**A**), IGF-1 (**B**), Ang-2 (**C**), FGF-2 (**D**), and PDGF-B (**E**) were evaluated by qPCR in RPE-choroid complexes of mice untreated or treated with vehicle or with UPARANT at 4 or 12 mg mL^{-1}. Data were analyzed by the formula $2^{-\Delta\Delta CT}$ using RpL13a as internal standard. Laser treatment increased angiogenic factors. UPARANT reduced them, with a trend toward recovering control levels ($^{*}P < 0.05$, $^{**}P < 0.01$, and $^{***}P < 0.001$ versus control; $^{\S}P < 0.05$, $^{\S\S}P < 0.01$, and $^{\S\S\S}P < 0.001$ versus vehicle-treated; ANOVA). Data are presented as scatter plots. Each plot represents the mean ± SEM of data from three independent samples, each containing one RPE-choroid complex.

Current anti-VEGF therapies used to counteract CNV in nAMD, although efficacious, require prolonged treatment regimens with frequent intravitreal injections and, consequently, carry some risks, potentially causing trauma and increasing the incidence of cataract, retinal detachment, hemorrhage, and endophthalmitis.[49] Interestingly, we have demonstrated that UPARANT administered by subcutaneous injection, a convenient and less invasive delivery route, particularly if considering long-term use of UPARANT, is as effective as intravitreal UPARANT in reducing VEGF levels, thus potentially inhibiting CNV (Supplementary Fig. S2). This indicates that the drug is taken up by the tissue from the administration site and is conveyed to the posterior segment of the eye by blood flow, resulting in a retinal concentration in the order of that reached after intravitreal administration.

UPARANT Mechanism of Action in CNV

In agreement with previous studies, the present findings demonstrate an increased expression of uPA and uPAR in the CNV model,[14,15] confirming a direct link between uPA/uPAR upregulation and choroidal angiogenesis. In this respect, uPA binding to uPAR causes extracellular matrix degradation, permissive for de novo development of blood vessels.[50] The fact that uPA upregulation involves both translational and posttranslational regulation hints at the existence of regulatory mechanisms distinct from transcriptional activation as putatively epigenetic mechanisms. In fact, several microRNAs have been demonstrated to regulate uPA expression in humans.[51,52] Upregulation of uPA/uPAR in CNV could be explained by presupposing that RPE and choroidal endothelial cells, both known to express uPA and uPAR,[13,14] may release soluble factors in response to the laser injury. Such factors could then exert activity in a paracrine fashion and increase the expression of uPA and uPAR, in turn representing the switch to induce choroidal angiogenesis.

Urokinase-type plasminogen activator receptor cross talk with FPRs plays a key role in physiological and pathologic processes, thus providing insights into the potential clinical relevance of new treatment regimens involving the uPAR/FPR system. As shown by the present results, laser treatment increases FPR2 proteins without affecting FPR1 and FPR3, indicating a prominent role of FPR2 in angiogenic processes.[19] In this respect, FPR2 agonism induces proliferation, migration, and tube formation in endothelial cells and promotes pathologic angiogenesis in in vivo models.[53] However, there is also evidence that FPR2 activation inhibits VEGF-induced neovascularization in a mouse model of corneal angiogenesis.[54] Nevertheless, in the specific case of the cornea, FPR2-mediated activation of angiogenesis-related transcription factors (HIF-1 and STAT3) could lead to upregulation of inhibitory Per/Arnt/Sim protein and soluble VEGFR,[55,56] both well characterized as responsible for the avascular phenotype of the cornea, by inhibiting VEGF-dependent neovascularization in the cornea.

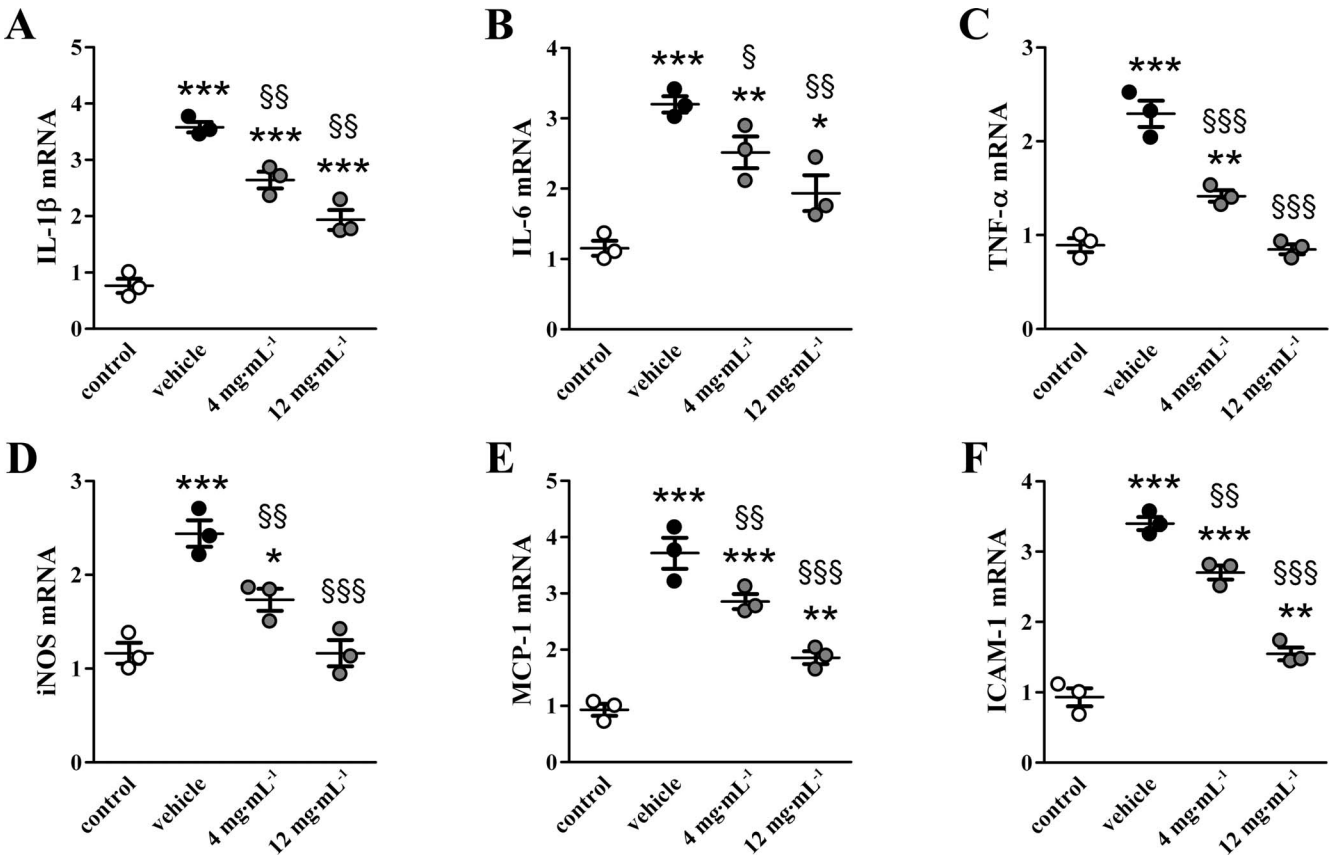

FIGURE 7. UPARANT reduces levels of inflammatory factors. Transcript levels of IL-1β (**A**), IL-6 (**B**), TNF-α (**C**), iNOS (**D**), MCP-1 (**E**), and ICAM-1 (**F**) were evaluated by qPCR in RPE-choroid complexes of mice untreated or treated with vehicle or with UPARANT at 4 or 12 mg mL^{-1}. Data were analyzed by the formula $2^{-\Delta\Delta CT}$ using RpL13a as internal standard. Laser treatment increased inflammatory factors. UPARANT reduced them, with a trend toward recovering control levels ($^{*}P < 0.05$, $^{**}P < 0.01$, and $^{***}P < 0.001$ versus control; $^{§}P < 0.05$, $^{§§}P < 0.01$, and $^{§§§}P < 0.001$ versus vehicle-treated; ANOVA). Data are presented as scatter plots. Each plot represents the mean ± SEM of data from three independent samples, each containing one RPE-choroid complex.

UPARANT has been designed to mimic the sequence ^{88}Ser-Arg-Ser-Arg-Tyr^{92}, through which uPAR interacts with and activates FPRs.[19] Accordingly, UPARANT competes with *N*-formyl-Met-Leu-Phe (fMLF), a known FPR ligand, for binding to FPRs. UPARANT excess prevents fMLF binding to FPRs, an indication that fMLF and UPARANT share the same binding site.[21] The present data demonstrating that UPARANT mitigates CNV by inhibiting HIF-1, STAT3, NF-kB, and CREB signaling pathways, even in the presence of elevated levels of uPA, suggest that UPARANT mitigates CNV by inhibiting FPRs-mediated regulation of transcription factors coupled to angiogenesis and inflammation.[19,20,57] Based on these facts, we propose a mechanism of action for UPARANT in CNV by preventing uPAR from activating the signaling cascade downstream of FPRs.

From a mechanistic point of view, an ischemic/inflammatory insult, as observed in AMD, activates several intracellular signaling pathways involved in promoting CNV. We hypothesize that, upon induction of CNV, uPA, uPAR, and FPR2 are upregulated, resulting in increased signaling downstream of the FPRs, leading to enhanced expression of angiogenic and inflammatory factors. Subsequently, upregulated soluble factors promote angiogenesis and inflammation, culminating in the pathologic state that characterizes CNV. Schematically, Figure 8 illustrates the complex molecular process through which UPARANT would act as an inhibitor of the interactions between uPAR and FPRs, thus ameliorating CNV.

UPARANT Effects on Angiogenesis and Inflammation

In the laser-induced CNV model of nAMD, the present results demonstrate that UPARANT reduces the expression of transcription factors, which are key regulators of the neoangiogenic response by mediating the production of both angiogenic and inflammatory factors. In particular, UPARANT action on HIF-1α and pSTAT3 described here is consistent with data obtained in a model of proliferative retinopathy in which UPARANT has been found to reduce their expression.[22] HIF-1 and STAT3 are two key regulators of VEGF expression.[58,59] In this respect, uPAR silencing downregulates VEGF expression by reducing the activity of both HIF-1 and STAT3 in glioma cells.[60] In addition, HIF-1 and STAT3 also regulate the expression of several inflammatory factors in line with a tight cross talk between angiogenesis and inflammation.[32] In this respect, the present results demonstrate that UPARANT almost normalizes the laser-induced upregulation of the transcription factors NF-kB and CREB that are known to control the expression of a large number of genes under inflammatory conditions.[61] Interestingly, the fact that either STAT3 or NF-kB may serve as a partner for HIF-1 in activating inflammatory pathways[62] suggests that cooperative relationships between transcription factors may participate in the pathogenesis of nAMD and indicates that UPARANT may

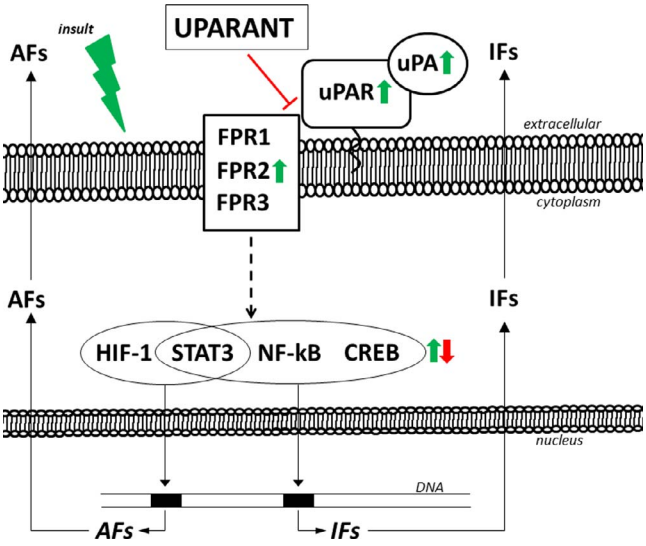

FIGURE 8. Schematic diagram of the intracellular pathways linking uPAR activation of FPRs to the production of angiogenic and inflammatory factors. An insult (e.g., an inschemic/inflammatory insult) upregulates uPA, uPAR, and FPR2, likely resulting in increased interactions between uPARs and FPRs. In turn, increased downstream FPR signaling increases the expression of angiogenic and inflammatory factors through the activation of transcription factors. Subsequently, upregulated soluble factors promote angiogenesis and inflammation, culminating in the pathologic state that characterizes nAMD. UPARANT would act as an inhibitor of these processes in preventing the interactions between uPARs and FPRs, thus ameliorating nAMD. *Green* schematics indicate upregulations, *red* schematics downregulations, *dashed* schematics multistep pathways. AF, angiogenic factors; IF, inflammatory factors.

suppress the cross talk between transcription factors involved in this pathology.

The present findings further confirm that nAMD, as many other ocular neovascular pathologies, is a multifactorial disease resulting from deregulation of several factors, including a variety of proinflammatory cytokines and chemokines. In nAMD, particularly, choroidal vessel growth is likely to be caused by either local tissue ischemia or the presence of an inflammatory reaction. However, a unifying model in which local inflammation triggers neovascularization is currently the most favored.[63] Accordingly, prevention of inflammation at early disease stages is sought as a therapeutic approach to avoid irreversible damage to the retinal tissue.

As a consequence of UPARANT-induced reduction of transcription factors, decreased levels of angiogenic and inflammatory markers have been determined in the choroid, thus indicating that uPA/uPAR/FPR activation may regulate their expression in response to ischemic/inflammatory insult and suggesting a causal relationship between the inhibitory effects of UPARANT and the amelioration of pathologic neovascularization (Fig. 8).

UPARANT, a Novel Therapy for AMD?

Previous and present data suggest that UPARANT may be potentially therapeutic for ocular diseases characterized by pathologic angiogenesis. In this respect, nAMD is characterized by largely irreversible vision impairment. In nAMD, CNV can be treated but not cured with VEGF inhibitors. In this respect, monthly injections of VEGF inhibitors are expensive to the health care system and burdensome to patients.[64] As compared to the currently used drugs, which act by abolishing VEGF bioavailability, here we demonstrate a novel mechanism through which increased levels of VEGF can be lowered. In fact, the present results highlight the finding that the levels of several angiogenic/inflammatory factors other than VEGF are reduced by UPARANT and that UPARANT treatment acts intrinsically by normalizing the upregulated levels of angiogenic/inflammatory factors. Taken together, these findings suggest that UPARANT treatment, by downregulating key transcription factors, thus normalizing a multitude of angiogenic and inflammatory molecules to basal levels, could avoid possible side effects deriving from the targeted inactivation of specific factors (e.g., anti-VEGF therapies) necessary for physiological responses, even during pathology.

CONCLUSIONS

The use of multitarget drugs may be an effective approach in the treatment of CNV. The present data provide evidence that the uPA/uPAR/FPR system and its interactome are promising targets for the development of antiangiogenic drugs against ocular angiogenesis. Although an extrapolation of these experimental findings to the clinic is premature, UPARANT may be viewed as a novel multitarget drug with potential implications for therapeutic interventions aimed at inhibiting the neovascular responses occurring in patients suffering from nAMD.

Acknowledgments

Supported by grants from Italian Ministero della Salute (RF-2011-02351158; PB; Roma, Italy), BIOOS Italia (PB; Montegiorgio, Italy); The Crown Princess Margareta Association for the Visually Impaired (HA; Valdemarsvik, Sweden), Edwin Jordan Foundation (HA; Stockholm, Sweden), Tore Nilsson Foundation (HA; Stockholm, Sweden), The Swedish Research Council (HA; Stockholm, Sweden), The Swedish Eye Foundation (HA; Umeå, Sweden); European Union–Fondi Europei per lo Sviluppo Regionale, Italian Ministero dell'Istruzione e dell'Università, and Italian Ministero dello Sviluppo Economico (PON01 02464; MDR and VP; Roma, Italy).

Disclosure: **M. Cammalleri**, None; **M. Dal Monte**, None; **F. Locri**, None; **L. Lista**, None; **M. Aronsson**, None; **A. Kvanta**, None; **D. Rusciano**, BIOOS (E); **M. De Rosa**, Pharmafelix (I, P); **V. Pavone**, Pharmafelix (I, P); **H. André**, None; **P. Bagnoli**, None

References

1. Resnikoff S, Pascolini D, Etya'ale D, et al. Global data on visual impairment in the year 2002. *Bull World Health Organ*. 2004; 82:844–851.
2. Miller JW. Age-related macular degeneration revisited—piecing the puzzle: the LXIX Edward Jackson memorial lecture. *Am J Ophthalmol*. 2013;155:1–35.e13.
3. Campochiaro PA. Molecular pathogenesis of retinal and choroidal vascular diseases. *Prog Retin Eye Res*. 2015;49:67–81.
4. Hytti M, Piippo N, Salminen A, Honkakoski P, Kaarniranta K, Kauppinen A. Quercetin alleviates 4-hydroxynonenal-induced cytotoxicity and inflammation in ARPE-19 cells. *Exp Eye Res*. 2015;132:208–215.
5. Izumi-Nagai K, Nagai N, Ozawa Y, et al. Interleukin-6 receptor-mediated activation of signal transducer and activator of transcription-3 (STAT3) promotes choroidal neovascularization. *Am J Pathol*. 2007;170:2149–2158.

6. Schmidt-Erfurth U, Chong V, Loewenstein A, et al. Guidelines for the management of neovascular age-related macular degeneration by the European Society of Retina Specialists (EURETINA). *Br J Ophthalmol*. 2014;98:1144–1167.
7. Lim JI, Fung AE, Wieland M, Hung D, Wong V. Sustained-release intravitreal liquid drug delivery using triamcinolone acetonide for cystoid macular edema in retinal vein occlusion. *Ophthalmology*. 2011;118:1416–1122.
8. Martin DF, Maguire MG, Fine SL, et al.; for Comparison of Age-related Macular Degeneration Treatments Trials (CATT) Research Group. Ranibizumab and bevacizumab for treatment of neovascular age-related macular degeneration: two-year results. *Ophthalmology*. 2012;119:1388–1398.
9. Nowak JZ. AMD–the retinal disease with an unprecised etiopathogenesis: in search of effective therapeutics. *Acta Pol Pharm*. 2014;71:900–916.
10. Amoaku WM, Chakravarthy U, Gale R, et al. Defining response to anti-VEGF therapies in neovascular AMD. *Eye (Lond)*. 2015; 29:721–731.
11. Todorich B, Yiu G, Hahn P. Current and investigational pharmacotherapeutic approaches for modulating retinal angiogenesis. *Expert Rev Clin Pharmacol*. 2014;7:375–391.
12. Uhrin P, Breuss JM. uPAR: a modulator of VEGF-induced angiogenesis. *Cell Adh Migr*. 2013;7:23–26.
13. Sugioka K, Kodama A, Okada K, et al. TGF-β2 promotes RPE cell invasion into a collagen gel by mediating urokinase-type plasminogen activator (uPA) expression. *Exp Eye Res*. 2013; 115:13–21.
14. Das A, Boyd N, Jones TR, Talarico N, McGuire PG. Inhibition of choroidal neovascularization by a peptide inhibitor of the urokinase plasminogen activator and receptor system in a mouse model. *Arch Ophthalmol*. 2004;122:1844–1849.
15. McGuire PG, Jones TR, Talarico N, Warren E, Das A. The urokinase/urokinase receptor system in retinal neovascularization: inhibition by A6 suggests a new therapeutic target. *Invest Ophthalmol Vis Sci*. 2003;44:2736–2742.
16. Rakic JM, Lambert V, Munaut C, et al. Mice without uPA, tPA, or plasminogen genes are resistant to experimental choroidal neovascularization. *Invest Ophthalmol Vis Sci*. 2003;44:1732–1739.
17. Eden G, Archinti M, Furlan F, Murphy R, Degryse B. The urokinase receptor interactome. *Curr Pharm Des*. 2011;17: 1874–1889.
18. Armbruster NS, Richardson JR, Schreiner J, et al. PSM peptides of *Staphylococcus aureus* activate the p38-CREB pathway in dendritic cells, thereby modulating cytokine production and T cell priming. *J Immunol*. 2016;196:1284–1292.
19. Prevete N, Liotti F, Marone G, Melillo RM, de Paulis A. Formyl peptide receptors at the interface of inflammation, angiogenesis and tumor growth. *Pharmacol Res*. 2015;102:184–191.
20. Cattaneo F, Guerra G, Ammendola R. Expression and signaling of formyl-peptide receptors in the brain. *Neurochem Res*. 2010;35:2018–2026.
21. Carriero MV, Bifulco K, Minopoli M, et al. UPARANT: a urokinase receptor-derived peptide inhibitor of VEGF-driven angiogenesis with enhanced stability and in vitro and in vivo potency. *Mol Cancer Ther*. 2014;13:1092–1104.
22. Dal Monte M, Rezzola S, Cammalleri M, et al. Antiangiogenic effectiveness of the urokinase receptor-derived peptide UPARANT in a model of oxygen-induced retinopathy. *Invest Ophthalmol Vis Sci*. 2015;56:2392–2407.
23. André H, Tunik S, Aronsson M, Kvanta A. Hypoxia-inducible factor-1α is associated with sprouting angiogenesis in the murine laser-induced choroidal neovascularization model. *Invest Ophthalmol Vis Sci*. 2015;56:6591–6604.
24. Kvanta A. Ocular angiogenesis: the role of growth factors. *Acta Ophthalmol*. 2006;84:282–288.
25. Shah RS, Soetikno BT, Lajko M, Fawzi AAA. A Mouse model for laser-induced choroidal neovascularization. *J Vis Exp*. 2015; doi:10.3791/53502.
26. Hollanders K, Van Bergen T, Van de Velde S, et al. Bevacizumab revisited: its use in different mouse models of ocular pathologies. *Curr Eye Res*. 2015;40:611–621.
27. Feng F, Cheng Y, Liu QH. Bevacizumab treatment reduces retinal neovascularization in a mouse model of retinopathy of prematurity. *Int J Ophthalmol*. 2014;7:608–613.
28. Liu H, Zhang W, Xu Z, Caldwell RW, Caldwell RB, Brooks SE. Hyperoxia causes regression of vitreous neovascularization by downregulating VEGF/VEGFR2 pathway. *Invest Ophthalmol Vis Sci*. 2013;54:918–931.
29. Wittchen ES, Nishimura E, McCloskey M, et al. Rap1 GTPase activation and barrier enhancement in RPE inhibits choroidal neovascularization in vivo. *PLoS One*. 2013;8:e73070.
30. Ijima R, Kaneko H, Ye F, et al. Interleukin-18 induces retinal pigment epithelium degeneration in mice. *Invest Ophthalmol Vis Sci*. 2014;55:6673–6678.
31. Hartsock A, Nelson WJ. Adherens and tight junctions: structure, function and connections to the actin cytoskeleton. *Biochim Biophys Acta*. 2008;1778:660–669.
32. de Oliveira Dias JR, Rodrigues EB, Maia M, Magalhães O Jr, Penha FM, Farah ME. Cytokines in neovascular age-related macular degeneration: fundamentals of targeted combination therapy. *Br J Ophthalmol*. 2011;95:1631–1637.
33. Yang SJ, Jo H, Kim JG, Jung SH. Baicalin attenuates laser-induced choroidal neovascularization. *Curr Eye Res*. 2014;39: 745–751.
34. Rennel ES, Regula JT, Harper SJ, Thomas M, Klein C, Bates DO. A human neutralizing antibody specific to Ang-2 inhibits ocular angiogenesis. *Microcirculation*. 2011;18:598–607.
35. Qu Y, Zhang S, Xu X, et al. Octreotide inhibits choroidal neovascularization in rats. *Ophthalmic Res*. 2009;42:36–42.
36. Zhang H, Yang Y, Takeda A, et al. A novel platelet-activating factor receptor antagonist inhibits choroidal neovascularization and subretinal fibrosis. *PLoS One*. 2013;8:e68173.
37. Xie P, Zhang W, Yuan S, et al. Suppression of experimental choroidal neovascularization by curcumin in mice. *PLoS One*. 2012;7:e53329.
38. Lavalette S, Raoul W, Houssier M, et al. Interleukin-1β inhibition prevents choroidal neovascularization and does not exacerbate photoreceptor degeneration. *Am J Pathol*. 2011;178:2416–2423.
39. She H, Nakazawa T, Matsubara A, et al. Reduced photoreceptor damage after photodynamic therapy through blockade of nitric oxide synthase in a model of choroidal neovascularization. *Invest Ophthalmol Vis Sci*. 2007;48:2268–2277.
40. Vlieghe P, Lisowski V, Martinez J, Khrestchatisky M. Synthetic therapeutic peptides: science and market. *Drug Discov Today*. 2010;15:40–56.
41. Urtti A. Challenges and obstacles of ocular pharmacokinetics and drug delivery. *Adv Drug Deliv Rev*. 2006;58:1131–1135.
42. Du H, Sun X, Guma M, et al. JNK inhibition reduces apoptosis and neovascularization in a murine model of age-related macular degeneration. *Proc Natl Acad Sci U S A*. 2013;110: 2377–2382.
43. Das A, McGuire P. Role of urokinase inhibitors in choroidal neovascularization. *Semin Ophthalmol*. 2006;21:23–27.
44. Koh HJ, Bessho K, Cheng L, et al. Inhibition of choroidal neovascularization in rats by the urokinase-derived peptide A6. *Invest Ophthalmol Vis Sci*. 2004;45:635–640.
45. Koh HJ, Freeman WR, Azen SP, et al. Effect of a novel octapeptide urokinase fragment, A6, on experimental choroidal neovascularization in the monkey. *Retina*. 2006;26:202–209.

Investigative Ophthalmology & Visual Science

46. Amadio M, Govoni S, Pascale A. Targeting VEGF in eye neovascularization: what's new?: a comprehensive review on current therapies and oligonucleotide-based interventions under development. *Pharmacol Res*. 2016;103:253–269.
47. van Lookeren Campagne M, LeCouter J, Yaspan BL, Ye W. Mechanisms of age-related macular degeneration and therapeutic opportunities. *J Pathol*. 2014;232:151–164.
48. Das RA, Romano A, Chiosi F, Menzione M, Rinaldi M. Combined treatment modalities for age related macular degeneration. *Curr Drug Targets*. 2011;12:182–189.
49. Janoria KG, Gunda S, Boddu SH, Mitra AK. Novel approaches to retinal drug delivery. *Expert Opin Drug Deliv*. 2007;4:371–388.
50. Montuori N, Ragno P. Role of uPA/uPAR in the modulation of angiogenesis. *Chem Immunol Allergy*. 2014;99:105–122.
51. Li C, Zhu HY, Bai WD, et al. MiR-10a and miR-181c regulate collagen type I generation in hypertrophic scars by targeting PAI-1 and uPA. *FEBS Lett*. 2015;589:380–389.
52. Li J, Kong F, Wu K, Song K, He J. Sun W. miR-193b directly targets STMN1 and uPA genes and suppresses tumor growth and metastasis in pancreatic cancer. *Mol Med Rep*. 2014;10: 2613–2620.
53. Lee MS, Yoo SA, Cho CS, Suh PG, Kim WU, Ryu SH. Serum amyloid A binding to formyl peptide receptor-like 1 induces synovial hyperplasia and angiogenesis. *J Immunol*. 2006;177: 5585–5594.
54. Leedom AJ, Sullivan AB, Dong B, Lau D, Gronert K. Endogenous LXA4 circuits are determinants of pathological angiogenesis in response to chronic injury. *Am J Pathol*. 2010; 176:74–84.
55. Makino Y, Cao R, Svensson K, et al. Inhibitory PAS domain protein is a negative regulator of hypoxia-inducible gene expression. *Nature*. 2001;414:550–554.
56. Ambati BK, Nozaki M, Singh N, et al. Corneal avascularity is due to soluble VEGF receptor-1. *Nature*. 2006;443:993–997.
57. Shin MK, Jang YH, Yoo HJ, et al. N-formyl-methionyl-leucyl-phenylalanine (fMLP) promotes osteoblast differentiation via the N-formyl peptide receptor 1-mediated signaling pathway in human mesenchymal stem cells from bone marrow. *J Biol Chem*. 2011;286:17133–17143.
58. Chen Z, Han ZC. STAT3: a critical transcription activator in angiogenesis. *Med Res Rev*. 2008;28:185–200.
59. Fong GH. Regulation of angiogenesis by oxygen sensing mechanisms. *J Mol Med*. 2009;87:549–560.
60. Malla RR, Gopinath S, Gondi CS, et al. Cathepsin B and uPAR knockdown inhibits tumor-induced angiogenesis by modulating VEGF expression in glioma. *Cancer Gene Ther*. 2011;18: 419–434.
61. Newton K, Dixit VM. Signaling in innate immunity and inflammation. *Cold Spring Harb Perspect Biol*. 2012;4(3): a006049.
62. Balamurugan K. HIF-1 at the crossroads of hypoxia, inflammation, and cancer. *Int J Cancer*. 2015;138:1058–1066.
63. Tezel TH, Bora NS, Kaplan HJ. Pathogenesis of age-related macular degeneration. *Trends Mol Med*. 2004;10:417–420.
64. Day S, Acquah K, Lee PP, Mruthyunjaya P, Sloan FA. Medicare costs for neovascular age-related macular degeneration, 1994–2007. *Am J Ophthalmol*. 2011;152:1014–1020.

Investigative Ophthalmology & Visual Science